

5. Venkatesan, T. R., Pande, K. and Gopalan, K., Did Deccan volcanism pre-date the Cretaceous/Tertiary transition? *Earth Planet. Sci. Lett.*, 1993, **119**, 181–189.
6. Sheth, H. C., Mahoney, J. J. and Chandrasekharam, D., Geochemical stratigraphy of Deccan flood basalts of the Bijasan Ghat section, Satpura Range, India. *J. Asian Earth Sci.*, 2004, **23**, 127–139.
7. Rama, S. N. I., Potassium–argon dates of some samples from Deccan Traps. Report of the 22nd International Geological Congress, New Delhi, 1964, Rep. 7, pp. 64–68.
8. Wellman, P. and Mc Elhinny, M. W., K–Ar ages of the Deccan traps, India. *Nature*, 1970, **227**, 595–596.
9. Kaneoka, I., Ar/Ar dating on volcanic rocks of the Deccan Traps, India. *Earth Planet. Sci. Lett.*, 1980, **46**, 233–243.
10. Alexander, P. O., Age and duration of Deccan volcanism: K–Ar evidence. *Mem. Geol. Soc. India*, 1981, **3**, 244–258.
11. Hofmann, C., Féraud, G. and Courtillot, V., $^{40}\text{Ar}/^{39}\text{Ar}$ dating of mineral separates and whole rocks from the Western Ghats lava pile: further constraints on duration and age of the Deccan traps. *Earth Planet. Sci. Lett.*, 2000, **180**, 13–27.
12. Knight, K. B., Renne, P. R., Halkett, A. and White, N., $^{40}\text{Ar}/^{39}\text{Ar}$ dating of the Rajahmundry Traps, eastern India and their relationship to the Deccan traps. *Earth Planet. Sci. Lett.*, 2003, **208**, 85–99.
13. Kerr, A. C., Khan, M., Mahoney, J. J., Nicholson, K. N. and Hall, C. M., Late Cretaceous alkaline sills of the south Tethyan suture zone, Pakistan: initial melts of the Réunion hotspot? *Lithos*, 2010; doi:10.1016/j.lithos.2010.02.010.
14. Widdowson, M., Pringle, M. S. and Fernandez, O. A., A post K–T boundary (Early Palaeocene) age for the Deccan-type feeder dykes, Goa, India. *J. Petrol.*, 2000, **41**(7), 1177–1194.
15. Duncan, R. A. and Pyle, D. G., Rapid eruption of the Deccan basalts at the Cretaceous/Tertiary boundary. *Nature*, 1988, **333**, 841–843.
16. Kent, R. W., Saunders, A. D., Kempton, P. D. and Ghose, N. C., Rajmahal basalts, eastern India: mantle sources and melt distribution in a rifted margin. In *Large Igneous Province: Continental, Oceanic and Planetary Volcanism*, Geophysical Monograph, American Geophysical Union, 1997, vol. 100, pp. 145–182.
17. Baksi, A. K., Ray Barman, T., Paul, D. K. and Farrar, E., Geochronological and geochemical studies of samples from Rajmahal and Sylhet traps, India; preliminary results. *EOS*, 1984, **65**, 303.
18. Ray, J. S., Pattanayak, S. K. and Pande, K., Rapid emplacement of the Kerguelen plume-related Sylhet Traps, eastern India: evidence from ^{40}Ar – ^{39}Ar geochronology. *Geophys. Res. Lett.*, 2005; DOI: 10.1029/2005GL022586.
19. Geological Survey of India, Geological map of Murwara Quadrangle, Madhya Pradesh. GSI, Hyderabad, 2004.
20. Melluso, L. and Sethna, S. F., Mineral compositions in the Deccan igneous rocks of India: an overview. In *Topics in Igneous Petrology* (eds Ray, J., Sen, G. and Ghosh, B.), Springer, Heidelberg, 2011, pp. 135–160.
21. Renne, P. R., Swisher, C. C., Deino, A. L., Karner, D. B., Owens, T. L. and DePaolo, D. J., Intercalibration of standards, absolute ages and uncertainties in $^{40}\text{Ar}/^{39}\text{Ar}$ dating. *Chem. Geol.*, 1998, **145**, 117–152.
22. Ludwig, K. R., Isoplot/Ex, v. 3.75, Berkeley Geochronology Center Special Publication No. 5, Berkeley, USA, 2012.
23. Kelley, S., Excess argon in K–Ar and Ar–Ar geochronology. *Chem. Geol.*, 2002, **188**, 1–22.
24. Chalapathi Rao, N. V., Burgess, R., Lehmann, B., Mainkar, D., Pande, S. K., Hari, K. R. and Bodhankar, N., $^{40}\text{Ar}/^{39}\text{Ar}$ ages of mafic dykes from the Mesoproterozoic Chhattisgarh basin, Bastar craton, Central India: implication for the origin and spatial extent of the Deccan Large Igneous Province. *Lithos*, 2011, **125**, 995–1004.
25. Lala, T., Chaudhary, A. K., Patil, S. K. and Paul, D. K., Mafic dykes of Rewa Basin, central India: implications on magma

dispersal and petrogenesis. In *Dyke Swarms* (ed. Srivastava, R. K.), Springer-Verlag, Berlin, 2011, pp. 141–162.

ACKNOWLEDGEMENTS. We thank the Department of Science and Technology, New Delhi for financial assistance to D.K.P. (No. ESS/16/213/2003) and to K.P. towards the development of the IIT Bombay–DST National Facility for Ar–Ar Geothermochronology. We also thank the anonymous reviewer for critical and constructive comments on the manuscript.

Received 21 January 2014; revised accepted 1 July 2014

Late Cretaceous diurnal tidal system: a study from Nimar Sandstone, Bagh Group, Narmada Valley, Central India

Biplab Bhattacharya* and Suparna Jha

Department of Earth Sciences, Indian Institute of Technology, Roorkee 247 667, India

Tidalites from the Cenomanian Nimar Sandstone, Bagh Group, Central India, are represented by (i) laterally accreted tidal bundles, (ii) herringbone cross-strata, (iii) sigmoidal cross-strata and (iv) tidal rhythmites with lenticular/wavy bedding. These indicate sedimentation in an upper subtidal to lower intertidal setting within fluvio marine interactive system. Time-series analysis of continuous rhythmic foreset bundles (sub-annual scale) manifests neap–spring tidal cycles within a diurnal tidal system with synodic and sidereal month lengths of ~28.4 lunar days and ~26.28 solar days respectively. Estimated Earth–Moon system parameters of the Late Cretaceous reveal no significant changes during the last ~100 Ma.

Keywords: Cenomanian, Cross-strata, lamina thickness, lunar orbital cyclicity, tidal bundles.

TIDALITES, represented by vertically accreted planar deposits (tidal rhythmites) and laterally accreted foreset bed forms (tidal bundles), within sandstone–mudstone heterolithic units preserve the records of past tidal activities. Analysis of the laterally and vertically continuous cyclic tidal successions provides an opportunity for precise estimation of lunar orbital periodicities and Earth–Moon parameters through geological ages^{1–3}. Biological chronometers, such as growth lines on corals and bivalves, have failed to come up as an alternative method for their lack of precision due to complex environmental and biogenetic factors⁴. Report of tidalites and interpretation of the corresponding Earth–Moon parameters is

*For correspondence. (e-mail: bbgeofes@iitr.ac.in)

available from the Precambrian^{5,6}, the Carboniferous^{3,7} and the Holocene⁸. The present study describes tide generated features from the Late Cretaceous and attempts to delineate the then Earth–Moon parameters.

Nimar Sandstone (Cenomanian, ~99.0–93.5 Ma), the basal unit of the Bagh Group in Narmada valley, Central India (Figure 1), has been well studied since long in terms of its rich content of fossil dinosaur bones, dinosaur egg shells, marine invertebrate body fossils and marine trace fossils⁹. The sedimentological aspects, however, have remained neglected so far, apart from some minor facies descriptions and report of some wave-generated primary sedimentary structures from selected localities^{10,11}. This communication describes various tidal bundles, including herringbone cross-strata, laterally accreted foresets with reactivation surfaces and mud drapes, climbing ripples, sigmoidal bundles, etc. and tidal rhythmites, viz. heterolithic pinstripe sand–mud laminae, wavy and lenticular bedding, etc. from the Nimar Sandstone in Narmada Valley. Thickness variation of foresets within the tidal bundles has been used here subsequently to quantify the lunar tidal periodicities and the Earth–Moon distance during the Late Cretaceous. Such records of the Earth–Moon parameters during the Cretaceous are not available till date.

Bagh Group of rocks (Cenomanian–Coniacian) in Central India is constituted of basal Nimar Sandstone (Cenomanian), overlain by Nodular Limestone (Turonian) and Coralline Limestone (Coniacian), and significantly bears records of Cretaceous marine transgression in Central India¹¹. The Bagh Group of sediments is undeformed, unmetamorphosed, nearly horizontal and

unconformably overlies the granite-granulites of the Precambrian Bijawar Group. These are commonly overlain by Deccan Trap volcanics (Late Cretaceous) in majority of the areas. Facies architecture of Nimar Sandstone (~35–40 m thick) depicts (i) an association of channel filling pebbly sandstone facies, lenticular conglomerate facies grading to sandstone and trough cross-stratified sandstone facies in the lower part, indicating a fluvial depositional system; (ii) followed upward by abundant sandstone–mudstone heterolithic facies with well-preserved tide- and wave-generated sedimentary features, intervened by multiple thin-bedded, trough, cross-stratified, sandstone facies, indicating a fluvio-marine interactive depositional system in the middle part, and (iii) an oyster-bearing sandstone facies intercalated with mudstone facies in the upper part of the succession, overlain by Nodular Limestone, indicating marginal marine depositional condition. The present study focuses on documenting the tide-influenced attributes within the sandstone–mudstone heterolithic facies from the Nimar Sandstone exposed in the Bagh River section and the Man River section near Bagh and Manawar areas respectively (Figure 1).

The sandstone–mudstone heterolithic facies (Figures 2 and 3) is represented by 2–25 cm thick sandstone beds alternating with 1–10 cm thick mudstone beds. Maximum thickness of this facies is up to 12 m in the Bagh area, where vertical cliffs exposed excellent sections of this facies. Individual sandstone beds are characterized by abundant ripple cross-laminae with development of bundled foresets (Figure 2 a–c). The shift from sand to mud is commonly gradational, whereas the contact between mud and overlying sand is abrupt. Foreset thickness and inclination vary laterally in cyclic pattern within one strata set (Figure 2 c). Foreset geometry often changes laterally from straight, truncating, to concave up with asymptotic toe, to sigmoidal. Different foresets are accreted laterally against prominent reactivation surfaces (Figure 2 a and c). Successive mud drapes on the sand foresets become flat and merge together in the bottom region, to produce thin mud veneers along the set boundaries (Figure 3 a). The abundance and thickness of mudstone drapes vary across the sets, showing an inverse relationship to the foreset thickness in sandstone: drapes are thinner and relatively rare in intervals of thicker foresets, while they are abundant and thicker in intervals of thinner foresets. Apparent bi-directional strata bundles in vertically adjacent sets are common (Figures 2 a–c and 3 a, b). Locally, preservation of individual ripple form with mutually opposite flow direction has led to development of herringbone cross-strata (Figures 2 a and 3 a). Climbing ripples are also common (Figure 2 b). Characteristically, majority of the ripple forms are often symmetrical in section and show well-rounded, broad crest with thin sand/mud drapes (Figure 2 b). Tidal rhythmites are developed within near-horizontal, centimetre thin sandstone–mudstone

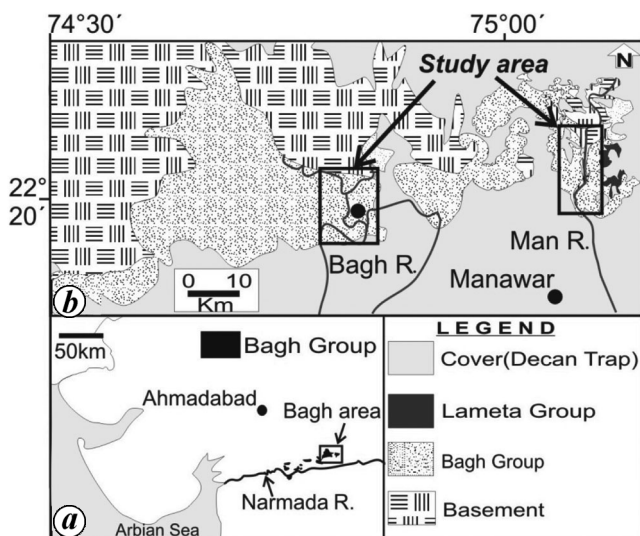


Figure 1. a, Geographic map showing the location of the Narmada Valley and the occurrence of the Bagh Group of rocks in peninsular India. b, Detailed geological map of the Bagh area showing occurrence of the Nimar Sandstone (modified after Khosla *et al.*⁹). The present study was carried out along the Bagh River and the Man River sections.

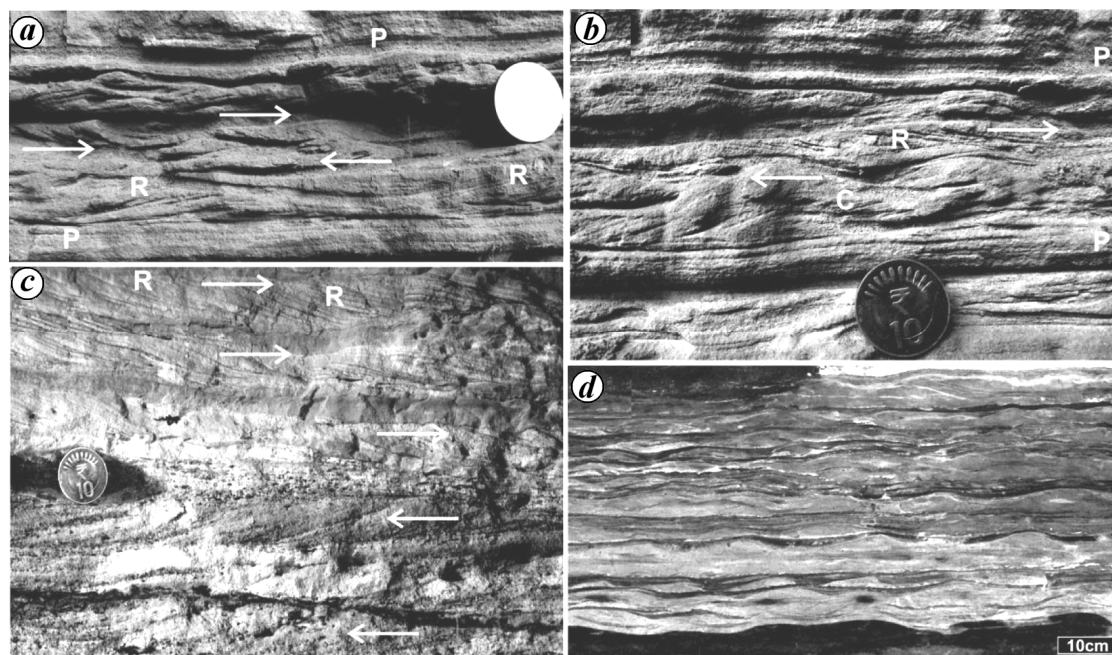


Figure 2. *a*, Mutually opposite cross-strata with preserved ripple forms within the sandstone beds of the sandstone–mudstone heterolithic facies. Lateral accretions of strata bundles against reactivation surfaces (R) are common. Note the presence of small sand drapes on ripple tops. *b*, Bi-directional strata bundles with development of small climbing ripples (C) and reactivation surfaces (R). Ripples show rounded, symmetrical crests. *c*, Cross-stratified sandstone showing mutually opposite foreset orientations in adjacent strata sets. *d*, Tidal rhythmites showing development of lenticular and wavy bedding. For (*a*–*c*), diameter of the coin is 2.5 cm and P represents plane lamination.

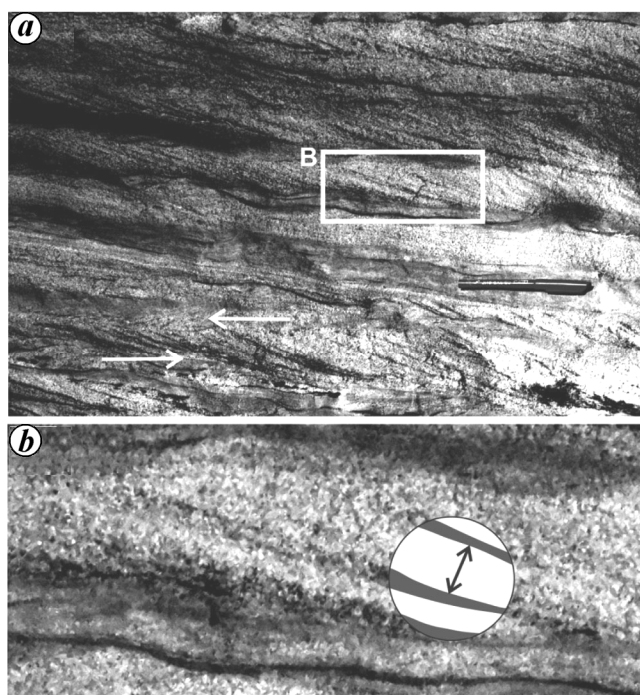


Figure 3. *a*, Vertically stacked tidal bundles showing alternate thickness cycles. Lamina thicknesses in each of the strata sets are measured. The portion within the white box is enlarged in (*b*). Note the development of herringbone cross-strata (arrows indicate apparent flow directions). *b*, Detailed view of tidal bundles. Thickness of the foreset is measured in a direction perpendicular to the foreset inclination (indicated by arrow).

alternations, commonly characterized by lenticular and wavy bedding (Figure 2 *d*), and multimetre-thin sand–mud alternations (pinstripe laminae), resembling inclined heterolithic strata (IHS).

Quantification of tidal cyclicity is based on the consideration that the variation of foreset thickness of tidal bundles is directly related to the tidal strength, which is dominantly controlled by lunar orbital periodicity and other Earth–Moon parameters¹². Lamina thickness is measured perpendicular to the dip of the foresets along a straight line between the upper and lower bounding surfaces (Figure 3 *b*). Lamina thickness measurements from these separate but laterally and vertically continuous cross-strata sets are plotted in lamina thickness versus lamina number plot (Figure 4 *a*), which indicates apparent cyclicity. To quantify the cyclicity and overcome any noise due to other natural influences or marine controls, a Fast Fourier transformation (FFT) is performed on a plot of approximately 252 continuous foresets (Figure 4 *b*). The data obtained are plotted in power spectral density versus frequency curves, which provide a cycle/event chain with one major peak corresponding to cyclicity value of 28.4 laminae/cycle and with several minor peaks having cyclicity values ranging between 1.15 and 0.83 lamina/cycle (Figure 4 *b*).

The studied sandstone–mudstone heterolithic facies is interpreted as tidal sediment due to the presence of (i) bundled sediment couplets (one sand foreset followed by

a mud drape) with lateral thickness variation, (ii) bipolar strata bundles with development of herringbone cross-strata, (iii) frequent reactivation surfaces, (iv) lenticular/wavy bedding and pinstripe heterolithic strata, which are the hallmark of tidal deposits^{13,14}. The sandstone–mudstone couplets indicate dominant tidal current followed by a slack phase between two successive tides^{13,14}. Frequent changes in tidal current intensity and direction are manifested by abundant reactivation surfaces (intermittent velocity asymmetry). Downcurrent changes in thickness and grain size across the laterally accreted strata bundles record systematic variation in tidal strength¹⁵. Sigmoidal bundles are generated by migration of linguoid ripples, formed at higher tidal flow velocity than the laterally accreted bundles^{15,16}. Low-angle topset that characterizes these cross-strata is also produced by migration of humpback ripples, in which the area between the crest point and the brink point represents a zone of non-flow separation, and flow separation occurs near the brink point¹⁶. Vertically accreted tidal bundles with thinly laminated sand–mud veneer indicate periodic flow fluctuations with sand-depositing traction current alternating with mud-depositing suspension sedimentation during quiescent phases. Alternate sand-dominant and mud-dominant units with variation in thicknesses of the sandstone foresets and mudstone drapes suggest alternate spring–neap–spring tidal cycles¹⁷. Bi-polar arrangements

of strata bundles with development of herringbone cross-strata indicate mutually opposite flow directions. Pre-dominance of sandstone beds over mudstone and abundance of mutually opposite cross-strata sets suggest deposition in subtidal channels. Locally, some horizons showing dominance of mudstone over sandstone with development of wavy/lenticular bedding suggest deposition in lower intertidal setting, which prevailed at certain phases during the depositional processes. Thus, an overall upper subtidal to lower intertidal set-up is inferred for the deposition of the studied tidalites. Ripples with rounded crests and symmetrical profiles with sand/mud drapes on top indicate reworking of these sediments by shallow-water waves.

The power spectral density plot of ~252 continuous laminae shows spectral periods of 28.4 events with thicker and thinner bundled sets corresponding to alternate neap and spring cycles, analogous to those derived from the modern tides and from the ancient records. The power spectra exhibit a consistent spectral period of ~1, which corroborates a dominantly diurnal tidal system with one tidal bundle developed by one dominant tidal current during a day. Absence of double mud drapes within the tidalites also manifests a diurnal tidal system. The upper cyclicity value of 28.4 indicates the number of tidal bundles within one cycle. Under diurnal system, each tidal bundle corresponds to a lunar day and thus, the number of days in one lunar (synodic) month during the Late Cretaceous is calculated as 28.4 days, which is less than the present-day value (29.53 days). However, spectral density plots of other discontinuous bundle sets (~112, ~83 and ~62 bundles) from the study area show varying periods between 30.4 and 27.5 laminae per cycle. We consider the value 28.4 laminae with an error level of ± 0.053 per cycle as more authentic, since under diurnal system 252 continuous tidal bundles represent the time-span between semi-annual and annual period³.

The lunar sidereal orbital period cannot be determined directly through measuring the lamina thickness. The present-day conversion value of $P_{\text{synodic}}/P_{\text{sidereal}}$ is 1.0808, whereas the same for Precambrian and post-Precambrian tidalites is ~1.069 to 1.07 respectively¹². Using $P_{\text{synodic}}/P_{\text{sidereal}}$ value as 1.07 (ref. 5) and applying the methodology proposed by Kvale *et al.*², the lunar sidereal month length during the Nimar sedimentation is calculated as $28.4/1.07 = 26.28$ solar days (present-day value is 27.32 days). Assuming that (i) the total length of the year has not changed significantly² from the present length of 31.56×10^6 sec and (ii) there is no secular change in the value of universal gravitational constant (g) throughout the geological time^{5,18}, the number of sidereal months in a year during the Cenomanian time is calculated as 13.9 (present-day value is 13.37 months/yr). Calculated length of the lunar sidereal month is intermediate between those calculated from the Archaean and the Proterozoic tidalites⁵. Using Kepler's third law of Earth–Moon

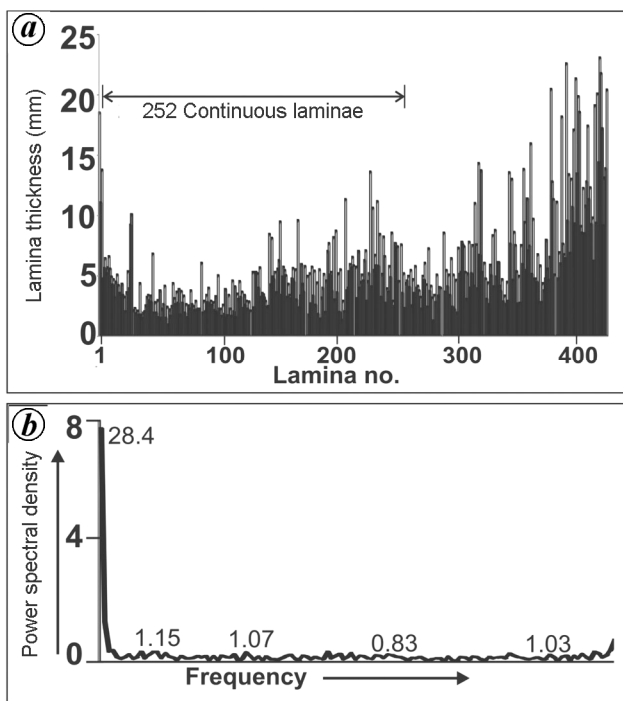


Figure 4. *a*, Lamina thickness versus lamina number plot showing rhythmic thickness variations in tidal bundles within the sandstone–mudstone heterolithic facies, Nimar Sandstone. *b*, Fast Fourier transformation power spectral–density plots of 252 continuous data presented in (*a*).

Table 1. Comparison of the synodic month lengths and the Earth–Moon orbital distances through geological ages

Age	Length of synodic month (lunar days)	Earth–Moon orbital distance	Data source
Present day	29.53	3.844×10^8 m	Kvale <i>et al.</i> ²
Late Cretaceous (Cenomanian)	28.4	3.7458×10^8 m	Present study
Pennsylvanian (~305 Ma)	29.17	Data not available	Kvale <i>et al.</i> ²
620 Ma	28.3	3.70×10^8 m	Williams ⁵
900 Ma	29.1	3.65×10^8 m	Sonett <i>et al.</i> ⁶
Palaeoproterozoic	32	Data not available	Mazumder and Arima ¹²
2450 Ma	31.1 ± 1.5	3.47×10^8 m	Williams ⁵

system, the relation between the lunar sidereal periods and the Earth–Moon distance is expressed as

$$(T_s/T_0)^2 = (d/d_0)^3, \quad (1)$$

where T_s and T_0 are the past and the present lunar sidereal periods (length of the lunar sidereal month) and d and d_0 are the Earth–Moon distances (semi-major axis of the lunar orbit) during the past and the present respectively. Considering the present length of the sidereal month (27.32 days) and the present Earth–Moon distance as 3.844×10^8 m, the Earth–Moon distance during ~99.0–93.5 Ma (Cenomanian) is calculated as 3.7458×10^8 m.

Using Kepler’s third law and following Coughenour *et al.*³, the total angular momentum of the Earth–Moon rotational system is expressed as

$$\begin{aligned} \omega_{\text{Total}} &= \omega_{\text{Earth}} + \omega_{\text{Moon}} = 2\pi I_E/T_S + 2\pi MR^2/T_m, \\ &= (0.5843 \times 10^{34}) + (2.854 \times 10^{34}) \text{ kg m}^2/\text{sec} \\ &= 3.4383 \times 10^{34} \text{ kg m}^2/\text{sec}, \end{aligned} \quad (2)$$

where I_E is the Earth’s moment of inertia = 8.034×10^{37} kg m², T_S the calculated length of sidereal day (Late Cretaceous) = 8.6397×10^4 sec, M the mass of moon = 7.3477×10^{22} kg, R the Cretaceous Earth–Moon orbital distance = 3.7458×10^8 m and T_m is the orbital period or length of the Cretaceous sidereal month = 2.27×10^6 sec (present-day value is 2.3606×10^6 sec).

The calculated angular momentum value is ~98.94% of the present-day value of the total angular momentum (3.475×10^{34} kg m²/sec) of the Earth–Moon system, indicating near-constant preservation of the angular momentum during the last ~100 Ma.

The nature and extent of tidal influence in relation to Late Cretaceous marine incursions in West-Central India is documented herein from a continental–fluvial to marginal marine transitional system. Preservation of mudstone-draped (pause plane) sandstone foresets, reactivation surfaces indicating time–velocity asymmetry, well-preserved bi-directional current flow patterns and alternate thick/thin-bedded sand-dominated and mud-dominated heterolithic units within the sandstone–mudstone heterolithic facies convincingly indicate deposition from tidal currents in the middle part of the Nimar Sandstone succession. Morphological similarity of the cross-strata bun-

dles with those described from the Permo-Carboniferous Talchir Formation¹⁶ and from Permian Barakar Formation¹⁵, suggests that these are produced by migration of sandwaves. Relative abundance of sandstone and mudstone (sand–mud ratio) and distribution of different primary structures indicate deposition in upper subtidal to lower intertidal conditions. Close intercalations of these sediments with fluvially derived trough cross-stratified sandstone facies attest to a transitional fluvio-marine interactive system that persisted during basal Bagh Group sedimentation. Gradual change in the facies architecture from a lower continental–fluvial to middle fluvio-marine, followed by marginal marine successions in the top suggests uninterrupted marine transgressions in the central peninsular India during the Late Cretaceous.

Well-preserved tidal bundles and tidal rhythmites within the Nimar Sandstone provide excellent scope for estimating the Earth–Moon system parameters during the Late Cretaceous. The calculated values of the Late Cretaceous synodic and sidereal months, the Earth–Moon distance and the angular momentum of the Earth–Moon system hold good when compared with other ancient records from Precambrian and younger stratigraphic sections world over (Table 1). The calculated values show marginal deviations in comparison to the present-day figures, which can be attributed to:

- (i) Partial modifications of the tidal bundles by other marine processes, viz. waves. Presence of shallow marine wave and its reworking is evident from the studied ripple geometry (discussed earlier).
- (ii) Partial reworking of the tidal sediments by fluvial processes under the fluvio-marine depositional systems.
- (iii) Human errors involved, including the errors in measurement of the lamina thickness, and missing or wrongly interpreting some of the laminae during measurements.
- (iv) Changing Earth–Moon distance through geologic time. Coughenour *et al.*³ enumerated that mean lunar retreat rate was ~1.46 cm/yr (with considerable error levels) since 315 Ma to the present. Comparing the calculated Earth–Moon distance during the Late Cretaceous (~99.0–93.5 Ma) with figure 6 of Coughenour *et al.*³ shows full conformity in terms of uniform Earth–Moon retreat during the last ~100 Ma.

1. Archer, A. W., Kuecher, G. J. and Kvale, E. P., The role of tidal velocity asymmetries in the deposition of silty tidal rhythmites (Carboniferous, Eastern Interior Coal Basin, USA). *J. Sediment. Res. A*, 1995, **65**, 408–416.
2. Kvale, E. P., Johnson, H. W., Sonett, C. P., Archer, A. W. and Zawistoski, A., Calculating lunar retreat rates using tidal rhythmites. *J. Sediment. Res.*, 1999, **69**, 1154–1168.
3. Coughenour, L. C., Archer, A. W. and Lacovara, J. K., Calculating Earth–Moon system parameters from sub-yearly tidal deposit records: an example from the carboniferous trade water formation. *Sediment. Geol.*, 2013, **295**, 67–76.
4. Berry, W. B. N. and Barker, R. M., Fossil bivalve shells indicate longer month and year in Cretaceous than present. *Nature*, 1968, **217**, 938–939.
5. Williams, G. E., Geological constraints on the Precambrian history of Earth's rotation and the Moon's orbit. *Rev. Geophys.*, 2000, **38**, 37–59.
6. Sonett, C. P., Kvale, E. P., Zakharian, A., Chan, M. A. and Demko, T. M., Late Proterozoic and Paleozoic tides, retreat of the Moon, and rotation of the Earth. *Science*, 1996, **273**, 100–104.
7. Archer, A. W. and Greb, S. W., Hyper tidal facies from the Pennsylvanian Period, Eastern and Western Interior Coal Basins, USA. In *Principles of Tidal Sedimentology* (eds Davis, R. A. and Dalrymple, R. W.), Springer, 2012.
8. Visser, R., Neap–spring cycles reflected in Holocene sub tidal large-scale bed form deposits: a preliminary note. *Geology*, 1980, **8**, 543–546.
9. Khosla, A. *et al.*, First dinosaur remains from the Cenomanian–Turonian Nimar Sandstone (Bagh Beds), District Dhār, Madhya Pradesh, India. *J. Paleontol. Soc. India*, 2003, **48**, 115–127.
10. Singh, S. K. and Srivastava, H. K., Lithostratigraphy of Bagh Beds and its correlation with Lameta Beds. *J. Paleontol. Soc. India*, 1981, **26**, 77–85.
11. Bose, P. K. and Das, N. G., A transgressive storm and fair weather wave dominated shelf sequence, Cretaceous Nimar Formation, Chakrud, Madhya Pradesh, India. *Sediment. Geol.*, 1986, **46**(1–2), 147–167.
12. Mazumder, R. and Arima, M., Tidal rhythmites and their implications. *Earth–Sci. Rev.*, 2005, **69**, 79–95.
13. Allen, J. R. L., Lower cretaceous tides revealed by cross-bedding with mud drapes. *Nature*, 1981, **289**, 579–581.
14. Terwindt, J. H. J., Origin and sequences of sedimentary structures in onshore mesotidal deposits of the North Sea. In *Holocene Marine Sedimentation in the North Sea Basin* (eds Nio, S. D., Shuttenhelm, R. T. E. and van Weering, T. J. C. E.), Special Publication No. 5, International Association of Sedimentologists, Blackwell Scientific Publications, Boston, 1981, pp. 4–26.
15. Bhattacharya, B., Bandyopadhyay, S., Mahapatra, S. and Banerjee, S., Record of tide wave influence on the coal-bearing Permian Barakar Formation. *Sediment. Geol.*, 2012, **267–268**, 25–35.
16. Bhattacharya, H. N. and Bhattacharya, B., A Permo-Carboniferous tide–storm interactive system, Talchir Formation, Raniganj Basin, India. *J. Asian Earth Sci.*, 2006, **27**, 303–311.
17. Greb, S. F. and Archer, A. W., Rhythmite sedimentation in a mixed tide and wave deposit: Hazel Patch Sandstone (Pennsylvanian) Eastern Kentucky Coalfield. *J. Sediment. Res. B*, 1995, **65**, 96–106.
18. Guenther, D. B., Krauss, L. M. and Demarque, P., Testing the constancy of the gravitational constant using helioseismology. *Astrophys. J.*, 1998, **498**, 871–876.

ACKNOWLEDGEMENTS. We thank the Department of Earth Sciences, IIT Roorkee, for providing infrastructural facilities. Constructive suggestions by anonymous reviewers are gratefully acknowledged.

Received 21 May 2014; revised accepted 4 July 2014

Natural base isolation system for earthquake protection

Srijit Bandyopadhyay¹, Aniruddha Sengupta^{1,*} and G. R. Reddy²

¹Department of Civil Engineering, Indian Institute of Technology, Kharagpur 721 302, India

²Structural and Seismic Engineering Section, Homi Bhabha National Institute, Mumbai 400 094, India

The performance of a well-designed layer of sand, geo-grid, geo-textiles and composites like layer of sand mixed with shredded tyre (rubber) as low-cost base isolators is studied in shake table tests in the laboratory. The building foundation is modelled by a 200 mm × 200 mm and 40 mm thick, rigid plexi-glass block. The block is placed in the middle of a 1 m × 1 m tank filled with sand. The selected base isolator is placed between the block and the sand foundation. Accelerometers are placed on top of the footing and foundation sand layer. The displacement of the footing is also measured by transducers. The whole set-up is mounted on the shake table and subjected to sinusoidal motion with varying amplitude and frequency. Sand is found to be effective only at very high amplitude (>0.65 g) of motion. Among all the different materials tested, the performance of a composite consisting of sand and 50% shredded rubber tyre placed under the footing is found to be the most promising as a low-cost, effective base isolator.

Keywords: Base isolation, earthquake protection, shake table test, shredded rubber tyre.

To find an economical and feasible way of designing new structures or strengthening existing ones for protection from damages during an earthquake is one of the challenges in civil engineering. The conventional approach to seismic hazard mitigation is to design structures with adequate strength and ability to deform in a ductile manner. Over the past two decades, newer concepts of structural vibration control, including seismic isolation, installation of passive and active/semi-active devices^{1–4} have been growing in acceptance. Traditionally, earthquake-resistant design of low- to medium-rise buildings is particularly important, as their fundamental frequencies of vibration are within the range where earthquake-induced force (acceleration) is the highest as found during the Mexico City Earthquake^{5,6}. One possible means to reduce the degree of amplification is to make the building more flexible⁷. In low to medium-rise buildings, this necessary flexibility can be achieved by the use of base isolation techniques. The primary mechanism for the reduction of shaking level in a base isolation method is energy dissipation.

*For correspondence. (e-mail: sengupta@civil.iitkgp.ernet.in)